Functional muscle recovery with nanoparticle-directed M2 macrophage polarization in mice

Theresa M. Raimondo[a,b] and David J. Mooney[a,b,1]

[a]John A. Paulson School of Engineering and Applied Sciences, Harvard University, Cambridge, MA 02138; and [b]Wyss Institute for Biologically Inspired Engineering, Harvard University, Boston, MA 02115

Edited by Robert Langer, MIT, Cambridge, MA, and approved September 4, 2018 (received for review May 4, 2018)

Persistence of inflammation, and associated limits in tissue regeneration, are believed to be due in part to the imbalance of M1 over M2 macrophages. Here, we hypothesized that providing a sustained source of an antiinflammatory polarizing cytokine would shift the balance of macrophages at a site of tissue damage to improve functional regeneration. Specifically, IL-4–conjugated gold nanoparticles (PA4) were injected into injured murine skeletal muscle, resulting in improved histology and an ∼40% increase in muscle force compared with mice treated with vehicle only. Macrophages were the predominant infiltrating immune cell, and treatment with PA4 resulted in an approximately twofold increase in the percentage of macrophages expressing the M2a phenotype and an approximately twofold decrease in M1 macrophages, compared with mice treated with vehicle only. Intramuscular injection of soluble IL-4 did not shift macrophage polarization or result in functional muscle improvements. Depletion of monocytes/macrophages eliminated the therapeutic effects of PA4, suggesting that improvement in muscle function was the result of M2-shifted macrophage polarization. The ability of PA4 to direct macrophage polarization in vivo may be beneficial in the treatment of many injuries and inflammatory diseases.

regenerative medicine | macrophage polarization | IL-4 | nanomedicine | muscle regeneration

Acute inflammation is a protective response that kills invading pathogens, should be self-limiting, and leads to healing. However, uncontrolled activation of immune cells, and failure of the acute inflammatory response to be self-limiting, leads to chronic inflammation, resulting in tissue damage (1). Following tissue injury or infection, monocytes (Mcs) are recruited from circulation and differentiate to M1 macrophages (Mφs), which promote inflammation by the release of inflammatory cytokines, reactive oxygen species, proteases, and antimicrobial peptides (2). Subsequently, Mφs adopt potent antiinflammatory and proregenerative activity, broadly referred to as M2 Mφs. Beyond antagonizing M1 responses, M1-to-M2 phenotype switching is important in promoting tissue regeneration and restoring homeostasis (2–4). M1–Mφ-dominated aberrant inflammation contributes to the pathogenesis of many chronic inflammatory conditions, including atherosclerosis, inflammatory bowel disease, asthma, rheumatoid arthritis, osteoarthritis, multiple sclerosis, and chronic venous leg ulcers (5–10). Hence, development of therapeutics that can dampen acute inflammation and promote M2 polarization are of considerable interest.

Mφ polarization plays a central role in directing skeletal muscle regeneration following injury (11, 12). Satellite cells, muscle resident stem cells, become activated to proliferate, migrate to the injury, fuse, and differentiate to form new myofibers (13, 14). Mφs directly control satellite-cell activation and maturation and are crucial to muscle regeneration (15, 16). M1 Mφs promote the proliferation of satellite and myogenic precursor cells, in vitro and in vivo, following human muscle injury, while M2 Mφs promote their differentiation (15). Imbalanced Mφ polarization, specifically skewing toward M1 phenotypes, has been shown to inhibit skeletal muscle repair (3, 16, 17). Transition to M2 phenotypes is critical to ultimately yield functional muscle (18).

The hypothesis underlying this study is that IL-4–conjugated gold nanoparticles (AuNPs) can direct M2a Mφ polarization, thereby enhancing regeneration of functional skeletal muscle following ischemic injury. IL-4 is an antiinflammatory cytokine that can induce the polarization of M1 Mφs toward the M2a state. Exogenous IL-4 is sufficient to drive accumulation of M2 Mφs through self-renewal, suggesting that IL-4 delivery can induce the expansion of therapeutic M2 Mφs without necessitating further recruitment of destructive M1 Mφs (19). IL-4 has been widely explored as a potential therapeutic in various inflammatory disease models, including autoimmune demyelinating disease, arthritis, and chronic skin inflammation (20–22). However, its use has required repeated infusions due to its short half-life in vivo. Resultant high-dose requirements and systemic side effects have limited the use of IL-4 treatments (23). Here, we utilize nanoparticles (NPs) for IL-4 delivery, as they allow distribution throughout the targeted tissue and can extend retention time compared with bolus delivery. AuNPs were specifically used because they can be synthesized with monodisperse size over a clinically relevant range (24), can be injected, and show minimal toxic or immunogenic activity in humans (25, 26). Formulations of gold (Au) are Food and Drug Administration-approved for the treatment of arthritis, a chronic inflammatory condition (27).

Results

Mφs Are Required for Regeneration of Muscle Function Following Ischemic Injury. We first explored the impact of Mc/Mφ depletion on spontaneous recovery from severe muscle damage. Ischemic injury of the left tibialis anterior (TA) muscle of C57BL6/J mice was induced by femoral artery/vein ligation. To deplete Mcs/Mφs, mice were treated starting 2 d before surgery

Significance

Chronic inflammation contributes to the progression of many diseases, including 7 of the 10 leading causes of death. Macrophages play a central role in regulating inflammation because they adopt proinflammatory (M1) and proregenerative (M2) phenotypes. While an initial M1 response is critical, the prolonged presence of M1 macrophages, or the imbalance of M1 over M2 macrophages, can cause tissue damage and inhibit regeneration. We demonstrate that gold nanoparticles can be used to deliver a cytokine to direct M2 macrophage polarization following muscle injury in vivo. The polarization shift promoted regeneration and increased muscle strength. The ability to direct macrophage polarization in an inflammatory microenvironment may be useful in the treatment of many injuries and inflammatory diseases.

Author contributions: T.M.R. and D.J.M. designed research; T.M.R. performed research; T.M.R. analyzed data; and T.M.R. wrote the paper.

The authors declare no conflict of interest.

This article is a PNAS Direct Submission.

[1]To whom correspondence should be addressed. Email: mooneyd@seas.harvard.edu.

This article contains supporting information online at www.pnas.org/lookup/suppl/doi:10.1073/pnas.1806908115/-/DCSupplemental.

Published online October 1, 2018.

with clodronate or PBS liposomes (Liposoma) as a control (Fig. 1*A* and *SI Appendix*, Fig. S1*A*). Clodronate treatment significantly reduced $CD45^+$ immune cell recruitment to the ischemic TA (Fig. 1*B*), due primarily to the depletion of myeloid cells (Fig. 1*C*). Flow cytometry showed a significant reduction in the percentage and absolute number of Mφs, Mcs, and Mcs/Mφs in the ischemic TAs following clodronate treatment, as expected (Fig. 1 *D–F* and *SI Appendix*, Fig. S1 *B–D*).

To determine if depletion of Mcs/Mφs inhibited recovery of TA function, TAs were stimulated ex vivo (*SI Appendix*, Fig. S2). A significant reduction in TA mass was observed on day 9 in mice treated with clodronate (*SI Appendix*, Fig. S1*E*). Although the overall weight of the mice was not affected, normalized TA mass was also significantly reduced with clodronate treatment (*SI Appendix*, Fig. S1 *F* and *G*). Ultimately, clodronate depletion of Mcs/Mφs resulted in significantly reduced TA contraction force and velocity following ischemic injury (Fig. 1 *G* and *H*).

Generation of NPs Presenting the Mφ Polarizing Cytokine IL-4. We next designed PEG-stabilized NPs presenting IL-4 to determine if promoting M2 polarization in damaged muscle could enhance recovery. First, it was demonstrated that soluble IL-4 shifted M1 Mφs to the M2 state in vitro (*SI Appendix*, Fig. S3). AuNPs were then synthesized by hydroquinone reduction of Au onto citrate-stabilized seed particles (24) and stabilized by partial PEGylation with 5-kDa PEG thiol (PEG-SH) (Fig. 2*A*). Subsequently, human or murine IL-4 was conjugated to the remaining Au surface (Fig. 2*B*). IL-4 conjugation likely occurred via thiol–Au bonds and electrostatic interactions. Dynamic light scattering (DLS) showed that AuNPs were monodisperse ∼30-, 60-, and 100-nm diameters with a slight right shift in size distribution following partial PEGylation and a second right shift following IL-4 conjugation (Fig. 2 *C–E* and *SI Appendix*, Fig. S4). ζ-potential was used to track surface modification of the AuNPs. Following

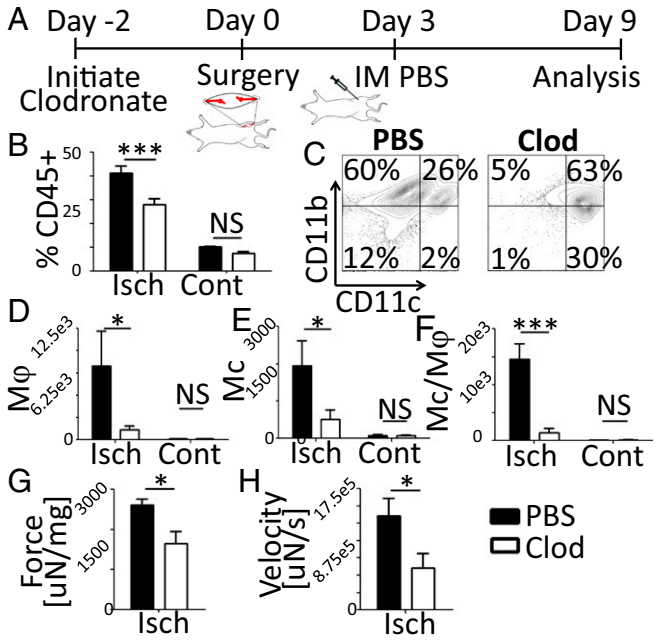

Fig. 1. Mcs/Mφs are required for regeneration of muscle function following ischemic injury. (*A*) Timeline showing clodronate treatment, injury, and injection to the ischemic TA. (*B*) Quantification of $CD45^+$ cells in the TA, day 9, flow cytometry data. (*C*) Gating of $CD45^+$ cells. (*D–F*) Number of Mφs ($CD11c^-/CD11b^+/Ly6G^-/Ly6C^-/F4/80^+$) (*D*), Mcs ($CD11c^-/CD11b^+/Ly6G^-/Ly6C^+/F4/80^-$) (*E*), and Mcs/Mφs ($CD11c^-/CD11b^+/Ly6G^-/Ly6C^+/F4/80^+$) (*F*) in the TA. (*G* and *H*) Maximum TA contraction force and velocity of three tests. Force was normalized to TA mass. Data are means ± SEM, $n = 7$. $^*P < 0.05$; $^{***}P < 0.001$; NS, not significant. Clod, clodronate; Cont, contralateral; Isch, ischemic.

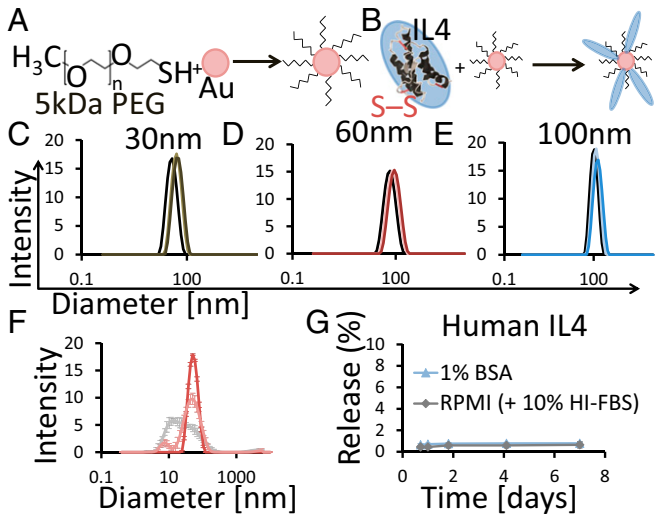

Fig. 2. AuNP Synthesis and human IL-4 conjugation. (*A* and *B*) Schematic showing partial PEGylation and subsequent IL-4 conjugation to AuNPs. (*C–E*) DLS size distribution of 30-nm (*C*), 60-nm (*D*), and 100-nm (*E*) AuNP core (black), AuNP-PEG (light color), and PA4 (dark color) particles. Data are from a representative synthesis. (*F*) PA4 DLS size distribution after IL-4 conjugation (dark pink) and after 1 d in RPMI + 10% HI-FBS at 37 °C (light pink). DLS distribution of RPMI + 10% HI-FBS (gray) is shown. Data are means ± SD, $n = 3$. (*G*) Thirty-nanometer-core PA4 were incubated at 37 °C, 5% CO_2 for 7 d, and the release of IL-4 into 1% BSA or RPMI + 10% HI-FBS was quantified with ELISA. Data are means ± SD, $n = 3$.

synthesis, 30- to 100-nm AuNP cores had ζ-potentials from −44 to −38 mV (measured in MilliQ water); following PEGylation and human IL-4 conjugation, the ζ-potentials became increasingly less negative, ranging from −10 to −15 mV for the 30- to 100-nm AuNP cores and −1.67 mV with murine IL-4 (*SI Appendix*, Table S1). IL-4 loading onto AuNPs was calculated based on subtractive analysis and compared with the theoretical maximum. The theoretical maximum was calculated based on sphere packing (*SI Appendix*, Fig. S5). IL-4 conjugation efficiency was fairly consistent for human and murine IL-4 and showed no statically significant differences across the 30- to 100-nm AuNP cores, representing ∼40–60% of the theoretical maximum (Table 1 and *SI Appendix*, Table S2). As the AuNPs were partially PEGylated, IL-4 conjugation efficiencies ∼50% were expected.

Stability of PEGylated, IL-4–conjugated particles (PA4) was assessed in vitro. Particle size was stable for 24 h in cell-culture conditions [37 °C, 5% CO_2, 10% heat-inactivated FBS (HI-FBS)], as there was no shift in PA4 size distribution over this time (Fig. 2*F*). AuNP-PEG was also stable in vitro (*SI Appendix*, Fig. S6*A*). Less than 1% of human IL-4 was released into complete RPMI medium or 1% BSA after 7 d, and only ∼3% of murine IL-4 was released after 61 d (Fig. 2*G* and *SI Appendix*, Fig. S6*B*).

PA4 Directs M2a Mφ Polarization. PA4 bioactivity was assessed in vitro with THP-1–derived human Mφs. An equivalent dose of soluble IL-4 (20 ng/mL) was used as a positive control and

Table 1. IL-4 conjugation

NP name	IL-4/nm^2	% of max. packing
100 nm PA4	0.075	50
60 nm PA4	0.065	43
30 nm PA4	0.061	41

Max., maximum.

AuNP-PEG as a negative control. PA4 and AuNP-PEG did not have a substantial effect on Mφ viability, even at 10× the IL-4 concentration used to polarize Mφs in vitro (*SI Appendix*, Fig. S7). While 100-nm-core AuNPs were slightly inflammatory, neither 30-nm-core PA4 nor AuNP-PEG induced the M1 state, even at concentrations 10× those used to polarize Mφs (*SI Appendix*, Fig. S8).

Importantly, PA4 up-regulated CD206 to the same extent as soluble IL-4, suggesting that conjugated IL-4 retained full bioactivity (Fig. 3*A* and *SI Appendix*, Fig. S8*A*). As expected, neither PA4 nor soluble IL-4 induced the expression of CD163 (Fig. 3*B* and *SI Appendix*, Fig. S8*B*), further supporting that PA4 specifically directed M2a polarization. There was no difference in the percentage of Mφs that adopted the M2a state between PA4 and soluble IL-4 treatments (Fig. 3*C*). Interestingly, the level of CD206 expression on M2a Mφs was significantly higher on those polarized with 30 nm, as opposed to 60- or 100-nm-core PA4 (Fig. 3*D*). This may relate to the greater volume and number of 30-nm-core particles in culture (*SI Appendix*, Table S3).

To determine if the stability of polarization driven by soluble IL-4 and PA4 was distinct, we replaced the initial soluble IL-4 or PA4 medium with basal medium after 1 d. A higher fraction of Mφs treated with PA4 retained M2a polarization (Fig. 3*E*). Furthermore, the level of CD206 expression on PA4-induced M2a Mφs was still elevated on day 5, while Mφs that had been polarized with soluble IL-4 demonstrated levels comparable to those in negative controls (Fig. 3*F*).

To determine if the multivalency of IL-4 presentation on PA4 contributed to the polarization effects, PA4 with varying degrees of IL-4 conjugation were made. Mφs polarized with PA4 with higher IL-4 valency demonstrated higher levels of M2a polarization (Fig. 3 *G* and *H*) and lower levels of the inflammatory state (Fig. 3*I*). All groups were treated with 20 ng/mL IL-4.

PA4 Enhances Muscle Fiber Regeneration and Contraction Force Following Ischemic Injury. Mice with ischemic hindlimbs were treated on day 3 with TA intramuscular (IM) injection of 2 μg of IL-4 as 30-nm-core PA4 or soluble IL-4, AuNP-PEG, or PBS and analyzed on days 6 and 15 (Fig. 4*A*). Immediately following surgery, blood flow was reduced by 60% in all conditions (*SI Appendix*, Fig. S9*A*). Ischemic injury also resulted in reduced TA mass on day 6, but was normalized by day 15 (*SI Appendix*, Fig. S9 *B* and *C*). Visual inspection revealed that AuNPs distributed throughout the TA, but not surrounding muscle, and were retained at least 3 d following injection (Fig. 4*B*).

To analyze the TA, we used H&E staining to quantify muscle fiber area and cell nuclei (28) (Fig. 4*C*). Immune cell infiltration was greater in TAs treated with PA4 compared with TAs treated with AuNP-PEG on day 6 (Fig. 4*D*). However, by day 15, immune-cell densities had decreased substantially in all groups (Fig. 4 *C* and *D*). Muscle-fiber area was significantly increased on day 15 in TAs treated with PA4 compared with AuNP-PEG (Fig. 4 *C* and *E*). Consistently, TAs treated with AuNP-PEG showed the greatest area of empty space (lacking muscle fibers or cell infiltration) compared with TAs treated with either soluble IL-4 or PA4 on day 15 (Fig. 4*F*).

Contraction force and velocity of damaged and treated TAs were analyzed on days 6 and 15 to assess function. Mass-normalized force and velocity were measured after tetanic stimulation (Fig. 4 *G* and *H*). Six days after induction of ischemia, mice in all treatment groups showed reduced muscle function, in comparison with the uninjured contralateral TA (*SI Appendix*, Fig. S10). By day 15, however, ischemic TAs treated with PA4 showed significant increases in contraction force of 1.4-fold compared with ischemic TAs treated with PBS and 1.6-fold compared with the contralateral TA. Treatment with bolus IL-4 or AuNP-PEG resulted in no improvement in force over mice treated with PBS. A similar trend was seen in contraction velocity. Improved TA function was not associated with improved blood perfusion, as perfusion was similar in all groups (*SI Appendix*, Fig. S11).

Mφs Are the Predominant Infiltrating Immune Cell Following Ischemic Injury. To probe the mechanism by which PA4 treatment improved muscle structure and function, we used flow cytometry to analyze cell recruitment and phenotype in the injured TA. As suggested by H&E, $CD45^+$ immune cells were cleared more rapidly following PA4 treatment compared with PBS (Fig. 5*A*). On day 15, the percentage of $CD45^+$ cells in the injured TA was elevated in the PBS group, but returned to levels comparable to those observed in the contralateral TA in the PA4 group (*SI Appendix*, Fig. S12*A*). Flow-cytometry data were normalized to

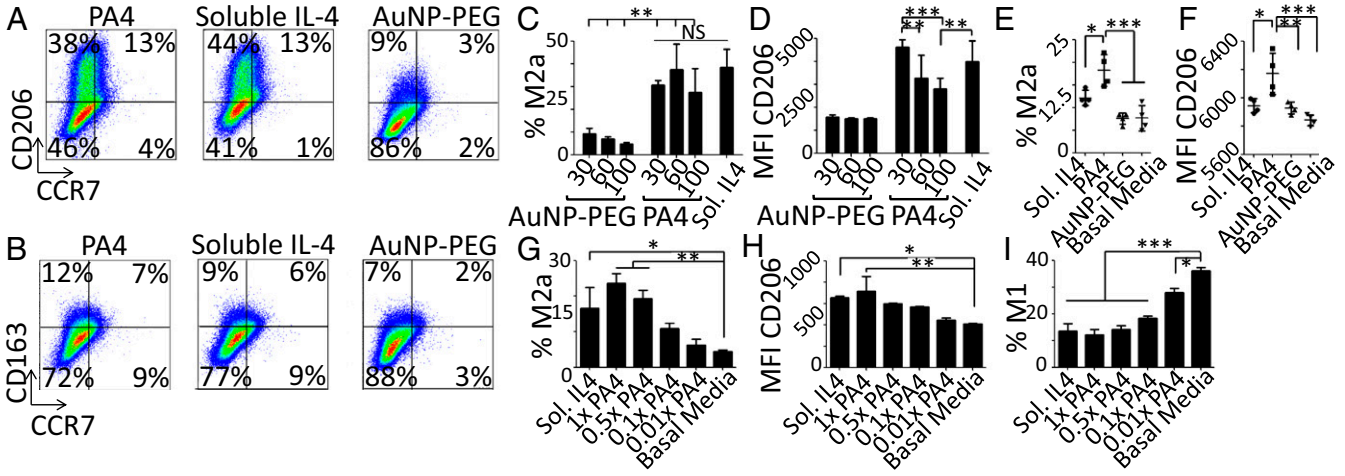

Fig. 3. PA4 directed M2a Mφ polarization. (*A* and *B*) THP-1 derived Mφs were treated for 3 d with 20 ng/mL IL-4 as 30-nm PA4 or soluble IL-4 or 30-nm AuNP-PEG. Plots show expression of the M2a (CD206) or M2c (CD163) vs. the M1 marker (CCR7). (*C*) Percentage of M2a ($CCR7^-/CD163^-/CD206^+$) Mφs. (*D*) CD206 median fluorescent intensity (MFI) within the $CD206^+$ gate. (*E* and *F*) Mφs were treated for 1 d with 20 ng/mL IL-4 as 30-nm PA4 or soluble IL-4, AuNP-PEG, or basal RPMI. On day 5, flow cytometry was used to quantify M2a ($CCR7^-/CD206^+$) Mφs. (*F*) CD206 MFI within the $CD206^+/CCR7^-$ gate. Data are means ± SD, $n = 4$. $^*P < 0.05$; $^{**}P < 0.01$; $^{***}P < 0.001$; NS, not significant. (*G–I*) Mφs were treated with 20 ng/mL IL-4 as soluble IL-4 or PA4 with varying degrees of IL-4 conjugation, 1×, 0.5×, 0.1×, and 0.01× (relative to the PA4s used throughout the work). (*G*) Flow cytometry was used to quantify M2a ($CD206^+/CCR7^-$) Mφs. (*H*) CD206 MFI within the $CD206^+$ gate. (*I*) Percentage of M1 ($CD206^-/CCR7^+$) Mφs. Data are means ± SEM, $n = 4$. $^*P < 0.05$; $^{**}P < 0.01$; $^{***}P < 0.001$ (Dunnett's comparison vs. basal media control).

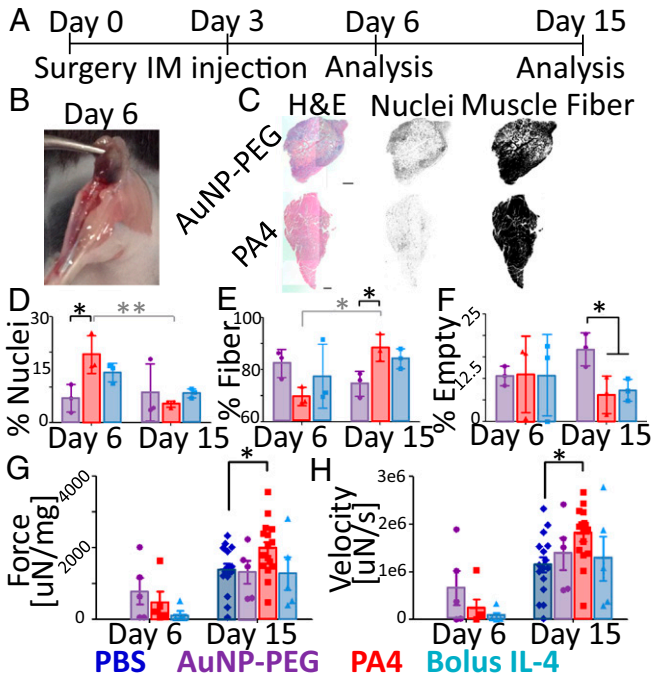

Fig. 4. PA4 enhanced muscle fiber regeneration and contraction force following ischemic injury. (*A*) Timeline showing surgery, treatment, and TA analysis. (*B*) Representative image showing the purple hue of AuNPs throughout the TA on day 6. (*C*) Representative H&E of ischemic TAs on day 15 hematoxylin (*Center*) and eosin (*Right*) channels. (Scale bars, 1.5 mm.) (*D*–*F*) Percentage of the TA cross-section associated with cell nuclei, muscle fibers, or empty area. Data are means ± SD, $n = 3$. $^*P < 0.05$; $^{**}P < 0.01$. Due to large variations in empty area on day 6, these data were excluded from statistics. (*G* and *H*) Maximum contraction force (25 V, 250 Hz) and velocity. Force was normalized to TA mass. Data are means ± SEM. Day 6, $n = 5$; day 15, $n = 16$ for PA4 and PBS, $n = 5$ for AuNP-PEG and bolus IL-4. $^*P < 0.05$ (Bonferroni planned comparison).

TA mass (*SI Appendix*, Fig. S12*B*). The same trend was seen in the mass of $CD45^+$ cells in the TAs (Fig. 5*B*). Recruited $CD45^+$ cells were characterized by expression of surface markers (*SI Appendix*, Fig. S12*C*). The level of Mcs in the injured TAs returned to levels comparable to that observed in the contralateral by day 6, and the level of Mφs returned to uninjured levels by day 15 in mice treated with PA4 (Fig. 5 *C* and *D*). Conversely, both Mcs and Mφs were still elevated on day 15 in the PBS group. PA4 treatment specifically reduced the level of inflammatory Mcs ($Ly6C^{hi}/Gr1^{lo}$) (Fig. 5*F*). Inflammatory Mcs were normalized to levels seen in the contralateral TA by day 6, while their presence was still elevated in the PBS group (Fig. 5*G*).

Although PA4 treatment resulted in more rapid clearance of immune cells, it did not alter the distribution of $CD45^+$ cells. The relative percentages of neutrophils, Mφs, Mcs, T cells, and patrolling Mcs were unaltered by PA4 treatment (*SI Appendix*, Fig. S12 *D*–*H*). These cell types followed patterns expected of a typical inflammatory response; neutrophils were present on day 3 and rapidly cleared, peak Mφ infiltration occurred on day 6, and patrolling Mcs were replenished on day 15. Importantly, however, Mφs were the predominant infiltrating immune cell, representing 42% on day 3 and 60% on day 6 of the $CD45^+$ cells (Fig. 5*E* and *SI Appendix*, Fig. S12*I*).

PA4 Enhances Muscle Regeneration by Directing M2a Mφ Polarization. To determine if PA4 treatment promoted a shift in Mφ phenotype away from the M1 and toward the M2a state, we assessed levels of CD206 (M2a) and CD80 (M1) expression (Fig. 6 *A*, *C*, and *E*). Approximately 20% of Mφs from TAs treated with PA4 expressed the M2a phenotype ($CD80^-/CD86^-/CD163^+/CD206^+$), but only ∼10% were M2a in the PBS group (Fig. 6*B*). Furthermore, mice treated with PA4 showed lower levels of M1 ($CD80^+/CD163^-/CD206^-$) Mφs on days 9–15 than mice treated with PBS (Fig. 6*D*). While both bolus IL-4 and PA4 reduced the percentage of $CD80^+$ Mφs on day 6, bolus IL-4 was as ineffective as AuNP-PEG at promoting the M2a state on day 15 (*SI Appendix*, Fig. S13).

To determine if the shift from the M1 toward the M2a state played a role in promoting muscle regeneration, we used clodronate to deplete Mφs before surgery. Following Mφ depletion and PA4 treatment, TA contraction force and velocity were reduced 1.9- and 2.8-fold, respectively, compared with mice that received PA4 treatment without Mφ depletion (Fig. 6 *F* and *G*). These data suggest that Mφs play a central role in the mechanism by which PA4 promotes functional muscle regeneration.

Discussion

The development of therapeutics that can control inflammation are of considerable interest, as failed resolution of inflammation and uncontrolled Mφ activation contribute to the progression of many diseases (1, 29). Here, we show that IL-4–conjugated AuNPs shift Mφs away from the M1 and toward the M2a state in vivo following ischemic skeletal muscle injury. PA4-driven Mφ polarization was more stable than that driven by soluble IL-4 in vitro and resulted in improved muscle-fiber regeneration and more rapid immune-cell clearance in vivo. Ultimately, PA4 treatment improved TA contraction force and velocity 2 wk following injury.

The findings of these studies demonstrate that Mcs/Mφs play a critical role in promoting muscle regeneration following ischemic

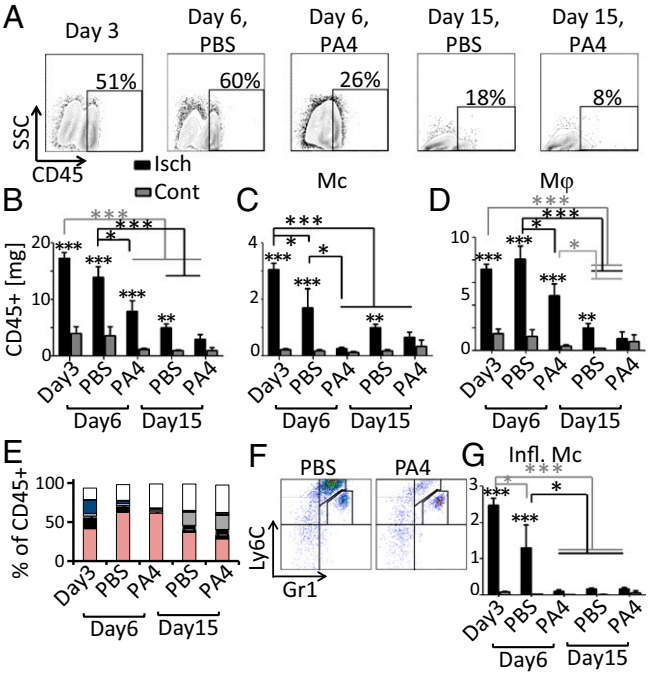

Fig. 5. Immune cells are cleared more rapidly following PA4 treatment. (*A*) Plots show the percentage of TA cells that were $CD45^+$. (*B*–*D*) $CD45^+$, Mcs ($CD45^+/CD11b^+/CD3^-/F4/80^-/Gr1^{lo\ or-}$), and Mφs ($CD45^+/CD11b^+/CD3^-/F4/80^+$) data normalized to TA mass (milligrams). (*E*) Distribution of $CD45^+$ cells in the TA: Mφs (pink; $CD11b^+/CD3^-/F4/80^+$), inflammatory Mcs (black; $Ly6C^{Hi}/Gr1^{Lo}$), Mcs (black above gray border; $Ly6C^{Hi}/Gr1^-$), patrolling Mcs (gray; $Ly6C^{Lo\ or-}/Gr1^-$), neutrophils (blue; $Ly6C^{Lo}/Gr1^{Hi}$), T cells (gray above the blue; $CD3^+$), and $CD11b^-/CD3^-$ (white). (*F*) Gating of myeloid ($CD45^+/CD11b^+/CD3^-/F4/80^-$) cells on day 6. Plots show diminishing inflammatory Mcs ($Ly6C^{Hi}/Gr1^{Lo}$) with PA4 treatment. (*G*) Inflammatory Mcs ($CD45^+/CD11b^+/CD3^-/F4/80^-/Gr1^{Lo}/Ly6C^{Hi}$) in TA normalized by mass (milligrams). Data are means ± SEM, $n = 5$–10. $^*P < 0.05$; $^{**}P < 0.01$; $^{***}P < 0.001$. Asterisks above columns indicate significance vs. contralateral. Cont, contralateral; Isch, ischemic.

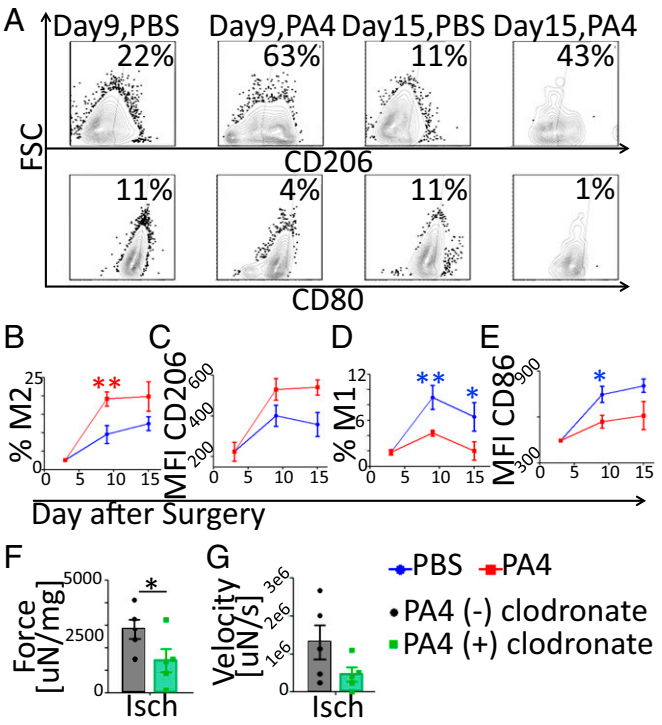

Fig. 6. PA4 enhanced muscle regeneration by directing M2a polarization. (*A*) Plots show the percentage of Mφs (F4/80$^+$/CD11b$^+$) from the ischemic TAs expressing CD206 (M2a) or CD80 (M1). (*B* and *D*) Percentage of Mφs expressing the M2 (CD80$^-$/CD86$^-$/CD163$^+$/CD206$^+$) or M1 (CD80$^+$/CD163$^-$/CD206$^-$) phenotype. (*C* and *E*) CD206 (M2a) or CD86 (M1) MFI. Data are means ± SEM, $n = 3$–5. $^*P < 0.05$; $^{**}P < 0.01$. (*F* and *G*) Mice were treated with either clodronate or PBS-liposomes and PA4. Maximum TA contraction force and velocity of three tests on day 9 are shown. Force was normalized to TA mass. Data are means ± SEM, $n = 5$. $^*P < 0.05$. Isch, ischemic.

injury. Mφs were the predominant infiltrating immune cell (Fig. 5*E*), and their depletion with clodronate inhibited regeneration of muscle contraction force and velocity (Fig. 1 *G* and *H*) and was coincident with a significant reduction in TA mass (*SI Appendix*, Fig. S1). This is in accord with previous reports that showed that Mc/Mφ depletion resulted in prolonged clearance of necrotic myofibers and increased muscle fat accumulation, and knockout of a Mφ chemotaxtic factor impaired histologic muscle regeneration (30, 31). Mφs have been shown to support myogenesis through the secretion of growth factors, and conditional deletion of the IGF1 gene in myeloid cells significantly impaired muscle regeneration (3). The interplay between Mcs/Mφs and myogenesis suggests that manipulation of Mφ function has the potential to improve muscle regeneration.

This study demonstrates that partial PEGylation of AuNPs, then IL-4 conjugation, yields monodispersed and stable PA4 for bioactive IL-4 delivery. AuNPs have been widely investigated for their use in drug delivery, as they provide a biologically inert, nonimmunogenic substrate (25, 26, 32, 33). Furthermore, by modifying surface chemistry, via PEGylation, their pharmacokinetics and in vivo biodistribution can be tuned (34). Partial PEGylation in this study allowed the subsequent conjugation of human and murine IL-4 directly to the remaining Au surface (Table 1 and *SI Appendix*, Table S2) and, importantly, resulted in PA4 that was stable in 10% serum in vitro (Fig. 2*F*) and following IM injection in vivo (Fig. 4*B*). PA4 showed no negative effects on Mφ viability in vitro. It was also not inflammatory and did not negatively affect blood perfusion (*SI Appendix*, Figs. S7, S8, and S11), TA weight, or contraction function in vivo (Fig. 4 and *SI Appendix*, Fig. S9). Importantly, conjugated IL-4 retained full bioactivity, as indicated by PA4-driven M2a polarization (Fig. 3). Mφs that had been polarized with PA4 expressed higher and more stable levels of CD206 than those polarized with soluble IL-4, and increasing IL-4 valency resulted in increasing levels of M2a polarization (Fig. 3 *E*–*H*). Various methods for delivery of IL-4 have been studied, including conjugation to decellularized scaffolds, encapsulation into mesoporous silica NPs, and the delivery of IL-4–encoding DNA in hyaluronic acid-poly(ethyleneimine) NPs (35–37). However, to date, these approaches have not resulted in therapeutic improvements in models of inflammation or injury. Conjugation of a targeting antibody to IL-4, in combination with dexamethasone, has shown therapeutic improvements in a murine arthritis model, but this approach may result in complications accompanying antibody therapy and require the development of new conjugation chemistries to target tissues affected by other diseases (38, 39). IL-4 conjugation to Au allowed for IM injection of nonimmunogenic PA4 into the ischemic muscle, providing a clinically relevant model to probe both their ability to direct Mφ polarization in an inflammatory microenvironment in vivo and the effects of Mφ polarization on therapeutic muscle regeneration.

PA4 treatment significantly enhanced functional muscle regeneration following ischemic injury. Inflammatory Mcs were cleared more rapidly (Fig. 5 *F* and *G*), and histologic muscle fiber regeneration (Fig. 4 *C*–*F*) and muscle contraction force and velocity were improved (Fig. 4 *G* and *H*) with PA4 treatment compared with negative controls. TAs treated with PA4 showed a 1.4- and 1.6-fold increase in contraction force and velocity, respectively, compared with muscles treated with PBS. Previous studies using mouse models of ischemic muscle injury reported comparable enhancements in muscle force 2 wk after delivery of growth factors and myogenic cells. In those studies, scaffold delivery of VEGF, IGF1, and/or myoblasts resulted in 1.5- to 3.0-fold increases in TA contraction force over control conditions (40–42). The present study suggests that similar functional improvements in muscle regeneration can be achieved by immune modulation with a single factor.

PA4 treatment enhanced muscle regeneration by directing M2a Mφ polarization. PA4 injection shifted the balance of Mφs away from the M1 and toward the M2a state (Fig. 6 and *SI Appendix*, Fig. S13). Treating TAs via IM injection on day 3 allowed the initial recruitment of M1 Mφs to occur, timing PA4 treatment with Mφ recruitment. Clodronate depletion of Mcs/Mφs before treatment with PA4 significantly diminished the recovery of TA contraction force and velocity (Fig. 6 *F* and *G*). This is consistent with previous findings that genetic deletion of microRNA-155, an RNA that does not regulate satellite cells but rather JAK-STAT signaling, and the balance between M1 and M2 Mφs, substantially delayed muscle regeneration (16). Other studies have shown that conditional deletion of the IGF1 gene or CREB-binding, both of which inhibit induction of the M2 state, severely inhibited muscle fiber regeneration (3, 17). M2 Mφs are critical for regeneration of functional muscle fibers, in part because they promote differentiation of myogenic precursor cells and formation of mature myotubes (15). In addition to directing M2a polarization, PA4 may have also directly affected myogenesis, as it has been shown that IL-4 directs myoblast fusion with myotubes (43). However, the loss of functional improvement following Mc/Mφ depletion in the present study suggests that directing Mφ phenotype is a key aspect of PA4 treatment. Furthermore, as it has been shown that IL-4 is capable of driving the accumulation of M2 Mφs through self-renewal (19), PA4 treatment may sustain M2a polarization via both the polarization of recruited M1 Mφs and through direct self-renewal of M2 Mφs.

The results of these studies indicate that IL-4–conjugated AuNPs can be used to direct M2a Mφ polarization in an inflammatory microenvironment following ischemic muscle injury in vivo. With the increasing realization that chronic inflammation plays a role in many diseases and that M2 Mφ polarization can potentially ameliorate many conditions, the ability of PA4 to direct Mφ polarization may be beneficial in the treatment of diverse conditions, including muscular dystrophies, inflammatory metabolic diseases like diabetes (44), and degenerative diseases.

Materials and Methods

For additional methods, see *SI Appendix*.

Surgery. Animal work was in compliance with National Institutes of Health and the Harvard Institutional Animal Care and Use Committee. Hindlimb ischemia was induced in female C57BL/6J mice (6–8 wk; Jackson Laboratories) by left unilateral femoral artery and vein ligation (40). On day 3, ischemic TAs were injected with 2 μg of IL-4 as PA4 or soluble IL-4, AuNP-PEG, or PBS; two 10-μL injections were given to each TA.

Mφ Depletion. Clodronate or PBS liposomes (Liposoma) were administered (*SI Appendix*, Fig. S1*A*).

Flow Cytometry. Cells from TAs and in vitro experiments were stained for surface markers of immune polarization.

TA Force. TAs were mounted ex vivo between electrodes (45). Three tetanic contractions were evoked. Contraction force, the difference between maximum force and baseline, was normalized to TA mass. Contraction velocity was the slope of the force curve at stimulation (*SI Appendix*, Fig. S2).

AuNP Synthesis. AuNPs were synthesized by hydroquinone reduction of Au onto citrate-stabilized seed particles (24).

PEG and IL-4 Conjugation. AuNP concentration was calculated with the Beer–Lambert Law. Partial PEGylation of AuNPs (5-kDa PEG-SH; Laysan Bio Inc) occurred overnight.

Subsequently, recombinant human or murine IL-4 (Peprotech) was conjugated in the presence of trehalose (Sigma catalog no. T0167). Subtractive analysis was used to quantify bound IL-4.

Histology. Images were tiled across the TA cross-section. To assess the percentage of the cross-section composed of muscle fibers (eosin) or nuclei (hematoxylin), ImageJ color deconvolution was performed.

Statistics. All analyses were performed on GraphPad Prism5. For experiments that involved more than one comparison, ANOVA with Tukey or Bonferroni post hoc test was used. Where noted, Dunnett's comparison vs. a control condition was used. For assessment of muscle function, a power analysis was performed on G*Power3.1 (46). PA4 and PBS groups were performed with $n = 16$ (per the analysis), and Bonferroni planned comparison was used.

ACKNOWLEDGMENTS. This work was supported by National Institutes of Health Grant DP3DK108224; the Wyss Institute for Biologically Inspired Engineering at Harvard University; and the National Science Foundation Graduate Research Fellowship Program (T.M.R.).

1. Kamaly N, et al. (2013) Development and in vivo efficacy of targeted polymeric inflammation-resolving nanoparticles. *Proc Natl Acad Sci USA* 110:6506–6511.
2. Murray PJ, Wynn TA (2011) Protective and pathogenic functions of macrophage subsets. *Nat Rev Immunol* 11:723–737.
3. Tonkin J, et al. (2015) Monocyte/macrophage-derived IGF-1 orchestrates murine skeletal muscle regeneration and modulates autocrine polarization. *Mol Ther* 23: 1189–1200.
4. Mantovani A, Biswas SK, Galdiero MR, Sica A, Locati M (2013) Macrophage plasticity and polarization in tissue repair and remodelling. *J Pathol* 229:176–185.
5. Mantovani A, Garlanda C, Locati M (2009) Macrophage diversity and polarization in atherosclerosis: A question of balance. *Arterioscler Thromb Vasc Biol* 29:1419–1423.
6. Zhang X, Mosser DM (2008) Macrophage activation by endogenous danger signals. *J Pathol* 214:161–178.
7. Kinne RW, Stuhlmüller B, Burmester GR (2007) Cells of the synovium in rheumatoid arthritis. Macrophages. *Arthritis Res Ther* 9:224–239.
8. Fahy N, et al. (2014) Human osteoarthritic synovium impacts chondrogenic differentiation of mesenchymal stem cells via macrophage polarisation state. *Osteoarthritis Cartilage* 22:1167–1175.
9. Mikita J, et al. (2011) Altered M1/M2 activation patterns of monocytes in severe relapsing experimental rat model of multiple sclerosis. Amelioration of clinical status by M2 activated monocyte administration. *Mult Scler* 17:2–15.
10. Sindrilaru A, et al. (2011) An unrestrained proinflammatory M1 Mφ population induced by iron impairs wound healing in humans and mice. *J Clin Invest* 121:985–997.
11. Kharraz Y, Guerra J, Mann C, Serrano A, Munoz-Canoves P (2013) Mφ plasticity and the role of inflammation in skeletal muscle repair. *Mediators Inflammation* 2013: 491497.
12. Tidball JG, Villalta SA (2010) Regulatory interactions between muscle and the immune system during muscle regeneration. *Am J Physiol Regul Integr Comp Physiol* 298: R1173–R1187.
13. Wagers AJ, Conboy IM (2005) Cellular and molecular signatures of muscle regeneration: Current concepts and controversies in adult myogenesis. *Cell* 122:659–667.
14. Engert JC, Berglund EB, Rosenthal N (1996) Proliferation precedes differentiation in IGF-I-stimulated myogenesis. *J Cell Biol* 135:431–440.
15. Saclier M, et al. (2013) Differentially activated macrophages orchestrate myogenic precursor cell fate during human skeletal muscle regeneration. *Stem Cells* 31:384–396.
16. Nie M, et al. (2016) MicroRNA-155 facilitates skeletal muscle regeneration by balancing pro- and anti-inflammatory macrophages. *Cell Death Dis* 7:e2261.
17. Ruffell D, et al. (2009) A CREB-C/EBPbeta cascade induces M2 macrophage-specific gene expression and promotes muscle injury repair. *Proc Natl Acad Sci USA* 106: 17475–17480.
18. Arnold L, et al. (2007) Inflammatory monocytes recruited after skeletal muscle injury switch into antiinflammatory macrophages to support myogenesis. *J Exp Med* 204:1057–1069.
19. Jenkins SJ, et al. (2011) Local macrophage proliferation, rather than recruitment from the blood, is a signature of TH2 inflammation. *Science* 332:1284–1288.
20. Racke MK, et al. (1994) Cytokine-induced immune deviation as a therapy for inflammatory autoimmune disease. *J Exp Med* 180:1961–1966.
21. Horsfall AC, et al. (1997) Suppression of collagen-induced arthritis by continuous administration of IL-4. *J Immunol* 159:5687–5696.
22. Ghoreschi K, et al. (2003) Interleukin-4 therapy of psoriasis induces Th2 responses and improves human autoimmune disease. *Nat Med* 9:40–46.
23. Zídek Z, Anzenbacher P, Kmonícková E (2009) Current status and challenges of cytokine pharmacology. *Br J Pharmacol* 157:342–361.
24. Perrault SD, Chan WC (2009) Synthesis and surface modification of highly monodispersed, spherical gold nanoparticles of 50-200 nm. *J Am Chem Soc* 131: 17042–17043.
25. Merchant B (1998) Gold, the noble metal and the paradoxes of its toxicology. *Biologicals* 26:49–59.
26. Root SW, Andrews GA, Kniseley RM, Tyor MP (1954) The distribution and radiation effects of intravenously administered colloidal Au198 in man. *Cancer* 7:856–866.
27. Ward JR, et al. (1983) Comparison of auranofin, gold sodium thiomalate, and placebo in the treatment of rheumatoid arthritis. A controlled clinical trial. *Arthritis Rheum* 26:1303–1315.
28. van Putten M, et al. (2010) A 3 months mild functional test regime does not affect disease parameters in young mdx mice. *Neuromuscul Disord* 20:273–280.
29. Serhan CN, et al. (2007) Resolution of inflammation: State of the art, definitions and terms. *FASEB J* 21:325–332.
30. Summan M, et al. (2006) Macrophages and skeletal muscle regeneration: A clodronate-containing liposome depletion study. *Am J Physiol Regul Integr Comp Physiol* 290:R1488–R1495.
31. Bryer SC, Fantuzzi G, Van Rooijen N, Koh TJ (2008) Urokinase-type plasminogen activator plays essential roles in macrophage chemotaxis and skeletal muscle regeneration. *J Immunol* 180:1179–1188.
32. Caster JM, Patel AN, Zhang T, Wang A (2017) Investigational nanomedicines in 2016: A review of nanotherapeutics currently undergoing clinical trials. *Wiley Interdiscip Rev Nanomed Nanobiotechnol* 9:e1416.
33. Yang X, Yang M, Pang B, Vara M, Xia Y (2015) Gold nanomaterials at work in biomedicine. *Chem Rev* 115:10410–10488.
34. Perrault SD, Walkey C, Jennings T, Fischer HC, Chan WC (2009) Mediating tumor targeting efficiency of nanoparticles through design. *Nano Lett* 9:1909–1915.
35. Spiller KL, et al. (2015) Sequential delivery of immunomodulatory cytokines to facilitate the M1-to-M2 transition of macrophages and enhance vascularization of bone scaffolds. *Biomaterials* 37:194–207.
36. Kwon D, et al. (2017) Extra-large pore mesoporous silica nanoparticles for directing in vivo M2 macrophage polarization by delivering IL-4. *Nano Lett* 17:2747–2756.
37. Tran TH, Rastogi R, Shelke J, Amiji MM (2015) Modulation of macrophage functional polarity towards anti-inflammatory phenotype with plasmid DNA delivery in CD44 targeting hyaluronic acid nanoparticles. *Sci Rep* 5:16632–16646.
38. Hemmerle T, Doll F, Neri D (2014) Antibody-based delivery of IL4 to the neovasculature cures mice with arthritis. *Proc Natl Acad Sci USA* 111:12008–12012.
39. Chames P, Van Regenmortel M, Weiss E, Baty D (2009) Therapeutic antibodies: Successes, limitations and hopes for the future. *Br J Pharmacol* 157:220–233.
40. Borselli C, et al. (2010) Functional muscle regeneration with combined delivery of angiogenesis and myogenesis factors. *Proc Natl Acad Sci USA* 107:3287–3292.
41. Borselli C, Cezar CA, Shvartsman D, Vandenburgh HH, Mooney DJ (2011) The role of multifunctional delivery scaffold in the ability of cultured myoblasts to promote muscle regeneration. *Biomaterials* 32:8905–8914.
42. Wang L, et al. (2014) Minimally invasive approach to the repair of injured skeletal muscle with a shape-memory scaffold. *Mol Ther* 22:1441–1449.
43. Horsley V, Jansen KM, Mills ST, Pavlath GK (2003) IL-4 acts as a myoblast recruitment factor during mammalian muscle growth. *Cell* 113:483–494.
44. Chawla A, Nguyen KD, Goh YP (2011) Macrophage-mediated inflammation in metabolic disease. *Nat Rev Immunol* 11:738–749.
45. Cezar CA, et al. (2016) Biologic-free mechanically induced muscle regeneration. *Proc Natl Acad Sci USA* 113:1534–1539.
46. Faul F, Erdfelder E, Lang AG, Buchner A (2007) G*Power 3: A flexible statistical power analysis program for the social, behavioral, and biomedical sciences. *Behav Res Methods* 39:175–191.